Enhancement of the crystallization of Tb_xFe_{1-x} thin films upon the formation of α-Tb phase

R. Ranchal [a,*], E. López [a], J.L. Prieto [b], C. Aroca [b]

[a] *Dpto Física de Materiales, Facultad CC. Físicas, Universidad Complutense de Madrid, Ciudad Universitaria s/n, Madrid 28040, Spain*
[b] *ISOM & Dpto Física Aplicada, ETSI Telecomunicación, Universidad Politécnica de Madrid, Ciudad Universitaria s/n, Madrid 28040, Spain*

Abstract

Tb_xFe_{1-x} thin films deposited by sputtering on Mo were investigated structurally and magnetically. The microstructure consists of $TbFe_2$ nanoparticles embedded in an amorphous matrix, and the Tb content can be correlated with an increase in the volume of these nanoparticles. Similar microstructure and behavior were found when $TbFe_2$ was deposited on glass and on a Pt buffer layer. Nevertheless, thermal treatments promote a different effect, depending on the mechanical stiffness of the buffer layer. The layers deposited on Mo, a rigid material, show crystalline $TbFe_2$ together with α-Tb phase upon thermal treatment. In contrast, $TbFe_2$ does not crystallize properly on Pt, a material with a lower stiffness than Mo. Intermediate results were observed on the film deposited on glass. Experimental results show the impact of the buffer stiffness on the crystallization process. Moreover, the formation of α-Tb appears to be fundamental to crystallized $TbFe_2$ on layers deposited on rigid buffers.

Keywords: Laves phase; Magnetostriction; Sputtering; Nanoparticles; Crystallization

1. Introduction

Crystalline $TbFe_2$ is the material with the highest magnetostriction at room temperature [1]. Layers deposited at room temperature by sputtering usually present an amorphous state which exhibits interesting properties, such as perpendicular magnetic anisotropy [2–8]. However, the inherent low reproducibility of this amorphous phase might be the reason behind the controversy about the physical origin of this anisotropy. As the magnetic properties do not appear to be completely reproducible in the amorphous state, investigations were focused on the crystalline $TbFe_2$ ordering, the one with potentially more magnetostriction. The crystalline Laves phase can be achieved either by means of post-growth annealing [9–14] or by heating the substrate during deposition [15,16]. The crystallization process on films deposited at temperature may depend not only on the temperature, but also on other parameters such as the gas pressure or the power during deposition. Therefore, it was decided to investigate this crystallization process on post-growth annealing. In a previous work, the effect of annealing on sputtered $TbFe_2$ thin films deposited at room temperature on different buffers and substrates was analyzed [14]. That investigation showed that the buffer layer has a stronger effect on the crystallization process than the substrate does, despite the former being much thinner. The experimental results could be understood by taking into account the stiffness of the buffer layer. Materials with a high Y/α parameter, where Y is Young's modulus, and α is the thermal expansion coefficient, seem to improve the crystallization process of $TbFe_2$ thin films.

This work presents further evidence on the role that stiffness of the buffer material plays on the crystallization process of the $TbFe_2$. The microstructure of Tb_xFe_{1-x} films with different compositions grown on Mo and of $TbFe_2$ deposited on glass and on Pt were studied thoroughly. In all cases, a microstructure composed of $TbFe_2$ nanoparti-

cles embedded in an amorphous matrix was found. Although the actual annealing temperature has little influence (within a range), high-quality $TbFe_2$ is better achieved by annealing samples deposited on a Mo buffer layer. The experimental results confirm the strong impact of the buffer stiffness on the crystallization process. Moreover, the formation of α-Tb appears to be pivotal to achieving crystalline $TbFe_2$ on layers deposited on rigid buffers.

2. Experimental techniques

Tb_xFe_{1-x} films were grown by a DC magnetron sputtering system at room temperature on Si substrates. Deposition was carried out from a single $TbFe_2$ commercial target in oblique incidence with an angle between the vapor beam and the perpendicular to the sample of ~25°. Different Ar pressures and DC power were used in order to achieve samples with slightly different compositions. Ar pressures ranged between 2×10^{-3} and 4×10^{-3} mbar, whereas the deposition power ranged between 60 and 120 W. The thickness of the Tb_xFe_{1-x} layers was 200 nm in all the samples. Mo buffer and capping layers were sputtered with power 90 W and Ar pressure 2×10^{-3} mbar, in order to avoid oxidation and promote crystallization [14]. Both, buffer and capping were 20 nm thick. Pt buffers, 20 nm thick, were also used for further investigations. Thermal treatments were mostly carried out at 400 °C in Ar atmosphere for 1 h. Additional annealing in the temperature range 300–500 °C was also performed for comparison. Energy dispersive X-ray spectroscopy was used to infer the sample composition. θ–2θ high-angle X-ray diffractometry was used to analyze the structural properties, while the magnetic characteristics were determined by means of a vibrating sample magnetometer at room temperature with the applied magnetic field parallel and perpendicular to the sample plane. The temperature dependence of the magnetization was characterized by means of SQUID magnetometry. Prior to measuring the temperature dependence of the magnetization, the sample was first cooled from room temperature to 5 K either under a saturation field of 2 kOe (field-cooled, FC) or at zero field (zero-field-cooled, ZFC). Then, FC and ZFC curves were recorded with an applied magnetic field of 100 Oe during the warm-up. Magnetization curves at 10 K were also recorded using SQUID.

3. Experimental results

3.1. As-grown Tb_xFe_{1-x} films deposited on Mo buffers

The as-grown samples show a small $TbFe_2$ diffraction peak (Fig. 1a), which rules out a complete amorphous structure in the studied samples. The intensity of this peak increases as the Tb content reaches 33%, i.e. $TbFe_2$ composition. Therefore, the X-ray diffraction (XRD) patterns show an improvement in the structural characteristics of the Tb_xFe_{1-x} films as the Tb content reaches the Laves phase. A wide peak centered around $2\theta = 32°$, which is related to the presence of an amorphous compound, is also observed.

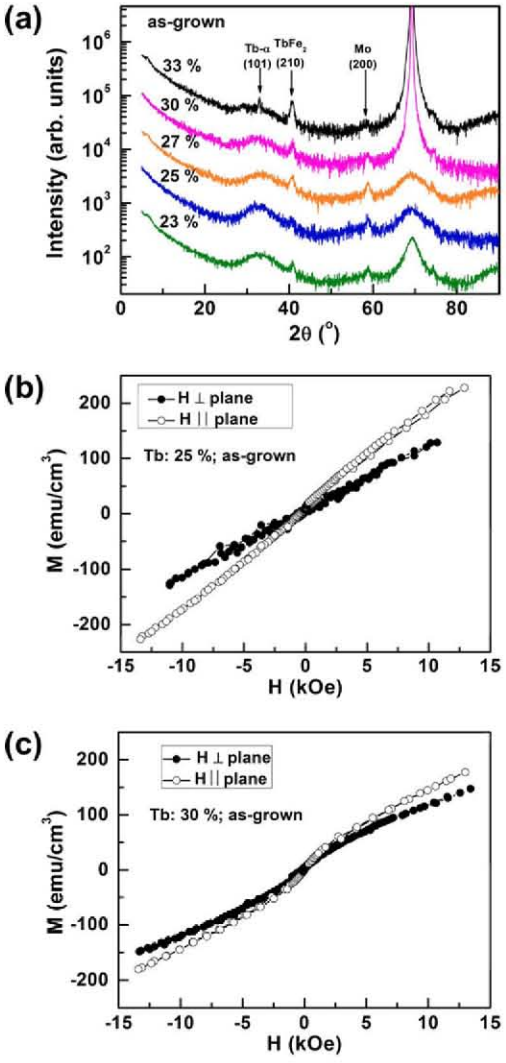

Fig. 1. (a) XRD patterns of Tb_xFe_{1-x} films with different Tb content. The Tb content is displayed on every curve. Curves are vertically shifted for clarity. (b and c) Room temperature magnetization curves of as-grown samples recorded with the applied magnetic field in the sample plane (○) and perpendicular to the sample plane (●) for samples with different Tb contents: (b) 25%; (c) 30%.

This broad peak is wider and more intense for the samples with a lower percentage of Tb, so it seems to be an amorphous compound rich in Fe (i.e. $TbFe_x$ with $x > 2$). Previous works showed that amorphous $TbFe_2$ generally exhibits out-of-plane magnetic anisotropy [2–8], but this magnetic characteristic is not observed in the present samples (Fig. 1b and c). This fact reinforces the authors' believe that the amorphous phase in the present samples is not $TbFe_2$, but a different Tb–Fe composition richer in Fe. This different behavior is most likely due to different deposition geometry in the sputtering system. The direction of the vapor beam during growth can drastically modify the direction of the anisotropy axis in Tb_xFe_{1-x} films [17]. In agreement with Muramatsu et al. [17], samples were obtained without out-of-plane anisotropy, as the incidence angle between the vapor beam and the perpendicular to the sample plane was 25°. The experimental results of this work show that the

absence of the perpendicular anisotropy might be related to the different microstructure of the layers studied in comparison with those of previous work where only an amorphous ordering was present in the $TbFe_2$ thin films [2–8].

Both, the in-plane and out-of-plane magnetization curves at room temperature exhibit a high saturation field and low coercivity, resembling the magnetic behavior of superparamagnets (Fig. 1b and c). This superparamagnetism could come from ferromagnetic $TbFe_2$ crystalline nanoparticles within the amorphous matrix, which could also justify the $TbFe_2$ peak in the X-ray measurements. This possibility was investigated through the dependence of the magnetization on temperature. Fig. 2a–c shows the FC and ZFC curves for as-grown layers with different Tb contents. The cusp in the ZFC curve is the so-called blocking temperature (T_B), and its presence reveals the existence of nanoclusters in all these samples deposited with a Mo buffer (Fig. 2a–c). The T_B can be used to determine the size of the nanoaggregates, taking into account the expression $kV = k_B T_B$, where K is the anisotropy constant, V is the crystallite volume, and k_B is the Boltzmann constant: 1.38×10^{-16} erg K^{-1}. The anisotropy is inferred using the expression $K = (\mu_0 H_K M_s)/2$, where H_K is the anisotropy field, i.e. the field necessary to saturate the hysteresis loop, and M_s is the saturation magnetization. Considering M_s, H_K and T_B for every sample, a correlation is obtained between the composition and the volume of the nanoaggregates (Fig. 2d). As the composition gets closer to $TbFe_2$ (i.e. 33% Tb), the volume of the nanoaggregates increases, a fact that is also visible in the X-ray measurements (an increase in the intensity of the $TbFe_2$ diffraction peak as the Tb content reached 33%). The hysteresis loops recorded at 10 K (insets to Fig. 2a–c) show a decrease in the magnetic moment as the Tb content increases. In order to calculate the value of M_s, m_s was divided by the total volume of the sample. Note that there is an uncertainty in the partial volume of $TbFe_2$ within the whole film, and therefore the calculated M_s should be lower than the real M_s for TbF_2. The calculated M_s for the sample with 33% is close to the $TbFe_2$ value (800 emu cm^{-3}), but for samples with a lower Tb content, higher M_s values are obtained than the bulk value for $TbFe_2$. This indicates that the amorphous TbFe matrix which contains the $TbFe_2$ nanoparticles is also contributing to the magnetic moment, as there is no sign of Fe or Tb isolated particles in the X-ray measurements. Finally, it is pointed out that this microstructure consisting of nanoaggregates embedded in an amorphous matrix was not reported in those previous works studying perpendicular magnetic anisotropy in amorphous Tb–Fe films [2–8]. Therefore, the different microstructure might be the reason behind the absence of out-of-plane magnetic anisotropy in the present samples.

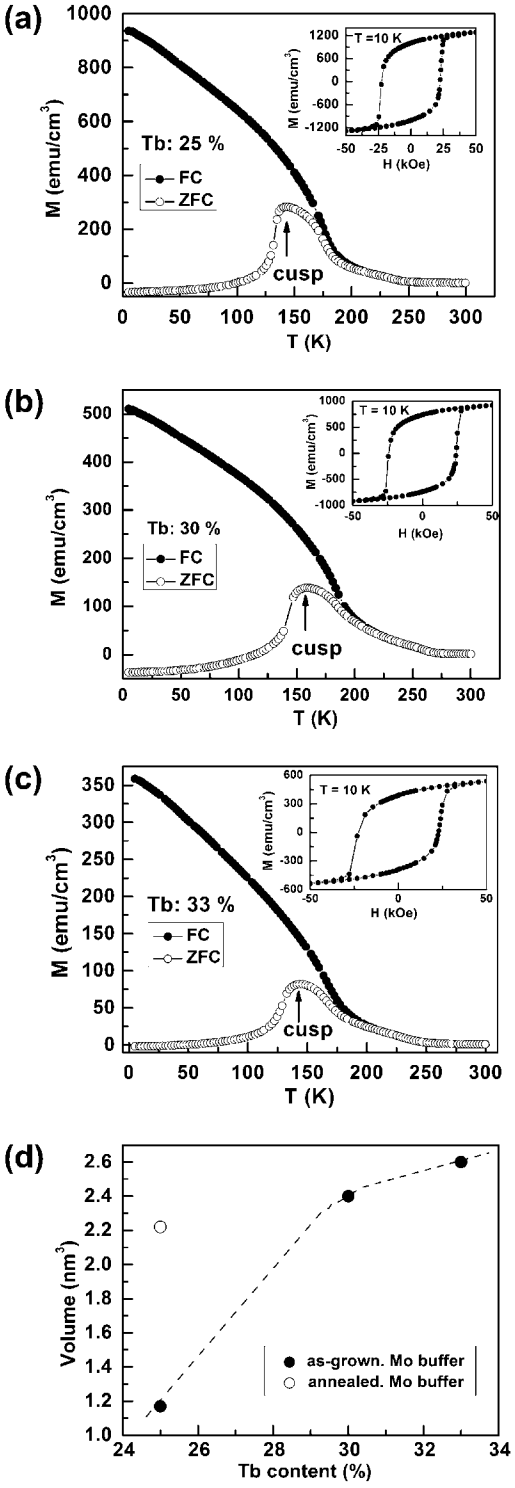

Fig. 2. FC (●) and ZFC (○) curves for Tb_xFe_{1-x} films with different Tb content: (a) 25%; (b) 30%; (c) 33%. In the inset of every graph is displayed the hysteresis loop of every sample recorded at 10 K. (d) Volume of nanoaggregates as a function of Tb content: (●) as-grown samples deposited on Mo buffers; (○) annealed samples deposited on Mo buffers.

3.2. *Annealed Tb_xFe_{1-x} films deposited on Mo buffers*

Fig. 3a shows the X-ray diffractometry of the samples annealed at 400 °C. Diffraction patterns reveal that the thermal treatment promotes not only the crystallization of the $TbFe_2$, but also the formation of the α-Tb phase. This Tb phase is highly polycrystalline, as indicated by the large number of different Tb diffraction peaks (Fig. 3b). Although a number of these peaks are present in all the samples, they

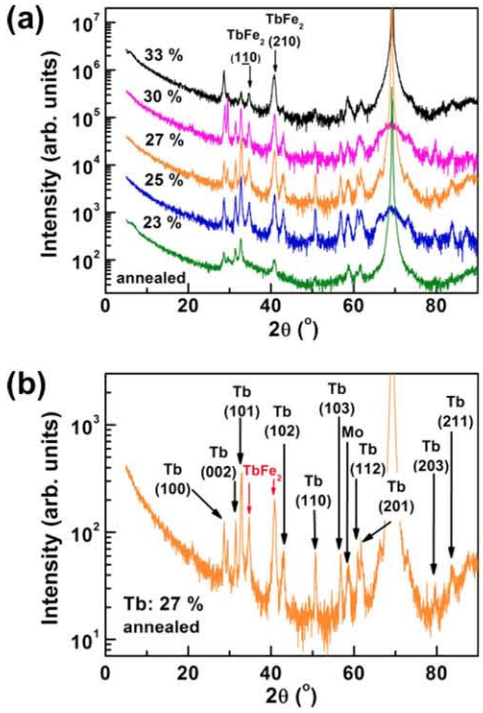

Fig. 3. (a) XRD patterns of Tb_xFe_{1-x} layers with different Tb content annealed at 400 °C. Only the $TbFe_2$ diffraction peaks are labeled. The Tb content is displayed in every curve, and they have been shifted for clarity. (b) XRD patterns of a Tb_xFe_{1-x} layer with a Tb content of 25% annealed at 400 °C. In this graph, all the peaks are labeled.

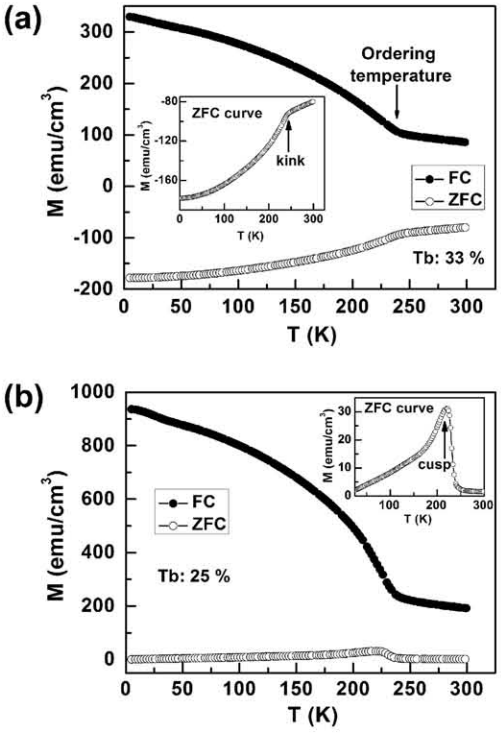

Fig. 4. FC and ZFC curves of an annealed Tb_xFe_{1-x} layer with a Tb content of (a) 33% and (b) 25%. Insets: detail of ZFC curve.

are clearly reduced for the stoichiometric content, i.e. 33% Tb.

The magnetic characterization shows that, for the annealed samples, the ZFC cusp is shifted to higher temperatures compared with the as-grown samples, and it eventually becomes a kink for a Tb content of 33% (Fig. 4a and b). The presence of a kink instead of a cusp in the ZFC curve indicates that the nanoaggregates have increased their volume, having almost disappeared upon thermal treatment. The increase in size for the $TbFe_2$ nanoaggregates means a decrease in volume in the amorphous matrix. Thus, the $TbFe_2$ sample could exhibit fewer α-Tb diffraction peaks than the rest of the samples because of the smaller volume of its annealed matrix. The FC and ZFC curves for the stoichiometric annealed sample show the presence of two different magnetic phases (Fig. 4a). The first has a Curie temperature (T_C) well above room temperature, as indicated by the large distance between the FC and ZFC curves at 300 K, and is quite likely to be crystallized $TbFe_2$ with a theoretical T_C of 700 K. This high T_C phase cannot be pure segregated Fe, as it does not show in the XRD patterns. The second magnetic phase that appears in the FC–ZFC curves has an ordering temperature ~240 K, very close to the T_C of the Tb (219 K). This is quite likely to be Tb with Fe impurities that might slightly increase its magnetic interaction.

Annealed samples with Tb contents <33% still show a cusp in the ZFC curves, and therefore the $TbFe_2$ nanoaggregates are still present. Similarly to the sample with 33% Tb, the FC–ZFC curves reveal a magnetic phase with $T_C > 300$ K, which corresponds to the crystallized $TbFe_2$ phase (Fig. 4b). Therefore, the thermal treatment has promoted crystallization in the samples with deficient Tb content, but the presence of nanoaggregates reveals that this crystallization is incomplete.

The influence of the temperature on the crystallization process was analyzed by performing thermal treatments in the temperature range 300–500 °C. There are diffraction peaks related to Tb for annealing temperatures as low as 300 °C (Fig. 5a), and no change was observed in the diffraction patterns as the annealing temperature increased. In agreement with the structural characterization, the shape of the hysteresis loops does not change with annealing temperature either (Fig. 5b). Therefore the annealing temperature is not a determining parameter for the formation of the α-Tb phase in Tb_xFe_{1-x} thin films.

3.3. $TbFe_2$ films deposited on glass substrates and on Pt buffers

A $TbFe_2$ film, i.e. with a 33% Tb content, was deposited directly onto a glass substrate and on a 20 nm thick Pt buffer in order to clarify the influence of the buffer on the crystallization process of $TbFe_2$ films (Figs. 6 and 7). Fig. 6 presents the magnetic characterization of the as-grown and annealed film deposited on the glass substrate. The as-grown sample exhibits a cusp in the ZFC curve (Fig. 6a) very similar to that observed in the layer grown

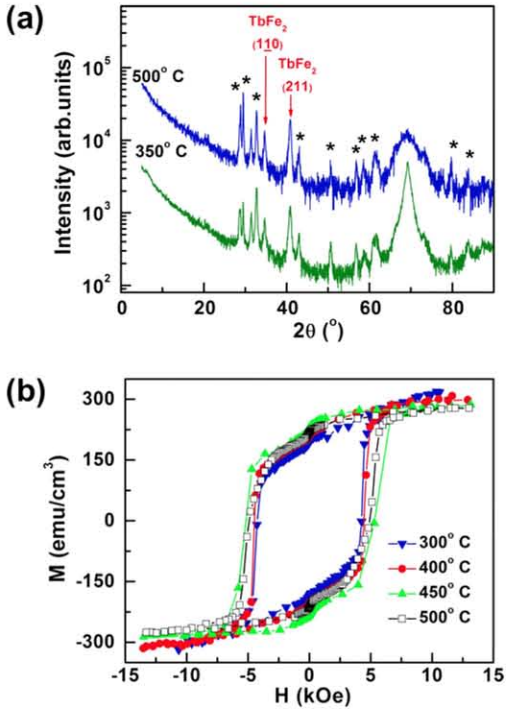

Fig. 5. (a) XRD pattern of a sample annealed at 300 °C and 500 °C. (b) Room temperature magnetization curves of TbFe films annealed at different temperatures: 300 °C (▼); 400 °C (●); 450 °C (▼); 500 °C (□).

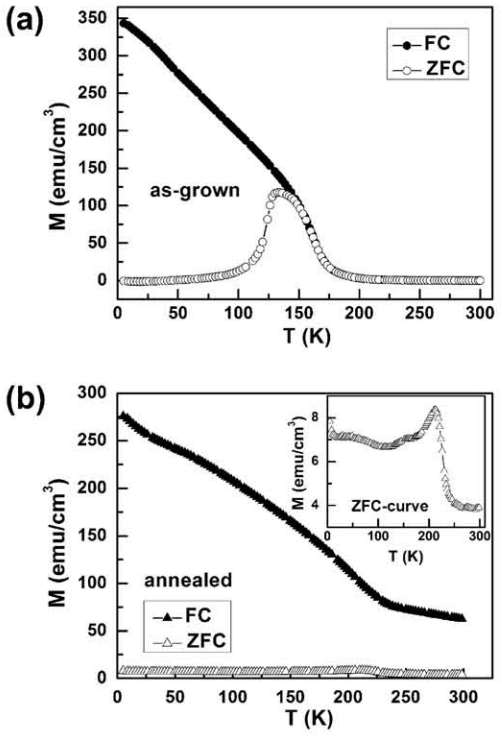

Fig. 6. FC and ZFC curves of a $TbFe_2$ thin film directly deposited on a glass substrate: (a) as-grown; (b) annealed at 400 °C.

on Mo. Moreover, the volume of the nanoaggregates is ~2.4 nm^3, almost equal to the value achieved for Mo. The annealed sample on glass also shows a ferromagnetic phase with T_C higher than room temperature, similar to

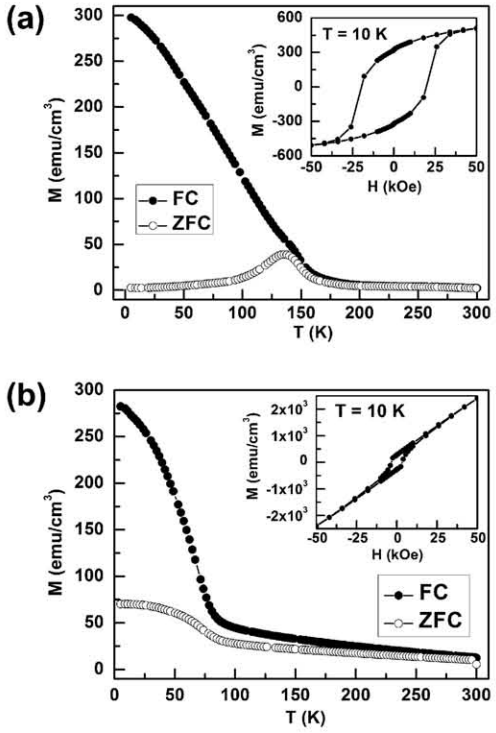

Fig. 7. FC and ZFC curves of a $TbFe_2$ thin film deposited on a 20 nm thick Pt buffer: (a) as-grown; (b) annealed at 400 °C. Insets: hysteresis loops at 10 K of (a) as-grown and (b) annealed samples.

the behavior observed in the layer on Mo (Fig. 6b). Nevertheless, the crystallization process is different for these samples. Whereas the ZFC cusp disappears in the annealed layer on Mo, the film deposited on glass still exhibits a ZFC cusp. A volume close to 10 nm^3 for the nanoaggregates left after the thermal treatment is inferred (Fig. 6b). Nevertheless, it is worth remarking on the relatively small ZFC cusp in the layer on glass, an indication of the almost complete crystallization process.

The magnetic characterization of the as-grown sample deposited on Pt shows a cusp in the ZFC curve (Fig. 7a), revealing the presence of nanoaggregates, as in the previous samples. The volume of the nanoaggregates (~3.5 nm^3) in the film grown on Pt is slightly higher than that obtained in samples with the same Tb content but deposited on Mo and glass. Moreover, the annealed sample deposited on Pt does not show the ZFC cusp, indicating the absence of nanoaggregates upon thermal treatment at 400 °C (Fig. 7b). Nevertheless, the FC–ZFC graph of this annealed layer is completely different from the others. First, a magnetic phase with an extremely low T_C of 70 K is present in the sample deposited on Pt (Fig. 7b). The origin of this magnetic phase might be an extremely low-quality $TbFe_2$. Secondly, the FC and ZFC curves are close together at temperatures ~300 K. Therefore, despite the absence of nanoaggregates in the annealed sample deposited on Pt, the $TbFe_2$ phase is not properly crystallized, as proved by the small distance between the FC and ZFC curves at 300 K. Moreover, the annealed $TbFe_2$ sample grown on Pt exhibits worse magnetic characteristics than non-stoichiometric annealed Tb_xFe_{1-x}

films grown on Mo. XRD patterns of the sample deposited on Pt have already been shown in previous work [14], and they show low structural quality. No clear diffraction peaks related to either $TbFe_2$ or α-Tb phase are present in those diffraction patterns.

4. Discussion

The crystallization of an amorphous material has two steps: (i) the formation of nucleation points (seeds); and (ii) their growth [18]. All the as-grown Tb_xFe_{1-x} films studied in this work exhibit the presence of nanoaggregates, whose volume depends on the Tb content of the sample, and it is optimum for a Tb content of 33%. However, despite the presence of nanoaggregates in all the samples, those deposited on Mo crystallize better than those deposited on glass or Pt, even if they have very similar characteristics before annealing. The present authors believe that the influence of the buffer layer on the crystallization of the $TbFe_2$ could be related to the stiffness of this buffer layer, as explained below. Previous work reported a qualitative estimation of the influence of the mechanical characteristics of the buffer layer on the magnetic and magneto-elastic properties of annealed $TbFe_2$ layers [14]. That work introduced a new mechanical parameter to take into account the substrate stiffness during thermal treatment: Y/α (see Section 1 of the present paper), which gets a higher value for "stiff" materials. It is remarked that that work ruled out other possible reasons such as the crystalline structure of the buffer or the substrate itself, and the only correlating parameter was the Y/α of the buffer material. In general, the volume of a material decreases during the transition from amorphous to crystalline [18]. Since the Tb_xFe_{1-x} films were deposited on a 20 nm thick Mo buffer layer, the extremely high Y/α factor of Mo (71×10^6 GPa K [14]) prevents, to a certain degree, a drastic volume change in the TbFe film during thermal treatment. Any crystalline phase that appears upon annealing will tend to minimize a volume change or the mechanical tensions induced. For instance, the crystallization of Tb is more likely than that of body-centered cubic (bcc) Fe, as the latter has a small lattice parameter (2.8664 Å),[1] and its nucleation would generate too much mechanical tension in the TbFe matrix. Therefore, when using a rigid buffer layer such as Mo, phases like Tb or $TbFe_2$ must be less costly energetically (less mechanical stress induced around), as their lattice parameters are larger, and the volume change in the transition from amorphous to crystalline must be smaller. In any case, when the $TbFe_2$ nanoaggregates grow in size during annealing, the system will try to compensate the change in volume somehow. This is done through the formation of a highly polycrystalline α-Tb phase: the amorphous TbFe phase segregates Tb during the thermal treatment to form the polycrystalline α-Tb phase, which is so obvious in the X-ray measurements, accommodating mechanical tensions in the structure. Of course, this process is more obvious in samples with more Tb, and that is why they crystallize better. Buschow and Dirks [19] already reported the presence of α-Tb in annealed $TbFe_2$ samples prepared by melt spinning. Therefore, the formation of α-Tb seems to play an important role in the crystallization of $TbFe_2$.

For the samples deposited on Pt, the picture is different. The low Y/α factor of the Pt (19×10^6 GPa K) allows a bigger volume change in the sample during annealing, and then the formation of $TbFe_2$ or α-Tb phase is not promoted so much. Therefore, although the $TbFe_2$ nanoaggregates are also present in the as-grown sample, they disappear upon thermal treatment. Moreover, in spite of the absence of nanoaggregates in the annealed sample, the magnetic characteristics are relatively low. Therefore, the experimental results point to close correlation between the formation of α-Tb and the proper crystallization of $TbFe_2$. A rigid buffer might enhance the segregation of Tb, promoting a better crystallization process. Glass has a Y/α factor of 45×10^6 GPa K, a value between those for Mo and Pt. The layer deposited on glass exhibits a ferromagnetic phase with a high T_C ($TbFe_2$), as indicated by the large distance between the FC and ZFC curves, although nanoaggregates with a volume close to 10 nm^3 are still present. Thus, the layer deposited on glass exhibits an intermediate crystallization process, in agreement with its intermediate mechanical stiffness in comparison with Mo and Pt. Degradation through interdiffusion does not appear to play an important role in the crystallization process. The film on glass crystallizes better than the layer deposited on Pt, although the oxidation process might potentially be enhanced in the former film.

5. Conclusion

Structural and magnetic investigations showed a phase separation of Tb_xFe_{1-x} films deposited by sputtering on Mo. The experimental results indicate the presence of $TbFe_2$ nanoparticles embedded in an amorphous matrix, and their volume depends on the Tb content. A similar microstructure is achieved in layers deposited on glass and on Pt buffers. Nevertheless, thermal treatments only promote optimum crystallization of the layers deposited on Mo. Those samples present not only the crystalline $TbFe_2$, but also a polycrystalline α-Tb phase. The large mechanical stiffness of Mo seems to play an important role, preventing volume change during annealing and therefore promoting phases with high lattice parameters, i.e. $TbFe_2$ and α-Tb. Experiments indicate that the formation of the Tb phase could be crucial for the crystallization process of $TbFe_2$.

Acknowledgements

This work was financially supported by the Spanish Ministry of Science through Projects MAT2008-02770/

[1] Lattice parameters: Mo, $a = b = c = 3.15$ Å; $TbFe_2$, $a = b = c = 7.3410$ Å; Tb-α, $a = b = 3.5990$ Å, $c = 5.6960$ Å; Fe (bcc), $a = b = c = 2.8664$ Å.

NAN and MAT2007-65965-C02. Universidad Complutense de Madrid (UCM) also partially supported this work through the "Consolidación de Grupos" program. The authors thank "CAI Difracción de rayos-X" of UCM for the X-ray diffractometry measurements and "CAI Técnicas Físicas" also of UCM for SQUID characterization.

References

[1] Clark AE, Belson HS. Phys Rev B 1972;5:3642.
[2] Lim SH, Choi YS, Han SH, Kim HJ, Shima T, Fujimori H. IEEE Trans Magn 1997;33:3940.
[3] Hellman F, Shapiro AL, Abarra EN, Robinson RA, Hjelm RP, Seeger PA, et al. Phys Rev B 1999;59:11408.
[4] Huang J, Prados C, Evetts JE, Hernando A. Phys Rev B 1995;51:297.
[5] Harris VG, Aylesworth KD, Das BN, Elam WT, Koon NC. Phys Rev Lett 1992;69:1939.
[6] Hellman F, Gyorgy EM. Phys Rev Lett 1992;68:1391.
[7] Hufnaget TC, Hellman F. J Magn Magn Mater 2003;256:322.
[8] Jiang HC, Zhang WL, Zhang WX, Peng B. Physica B 2010;405:834.
[9] Clark AE. Appl Phys Lett 1973;23:642.
[10] Wakiwaka H, Yamada Y, Watanabe T, Umemoto Y, Kiyomiya T, Makimura M. Int J Appl Electromagn Mech 2001;14:435.
[11] Innoue M, Fujii T, Gibb MRJ. IEEE Trans Magn 1996;32:4758.
[12] Zhang WL, Jiang HC, Zhang JP, Zhang WX. J Magn Magn Mater 2004;284:128.
[13] Jiang H, Zhang W, Zhang W, Yang S, Zang H. J Mater Sci Technol 2005:21,315.
[14] Ranchal R, Prieto JL, Sánchez P, Aroca C. J Appl Phys 2010;107:113918.
[15] Wang CT, Osgood III RM, White RL, Clemens BM. Mater Res Soc Symp Proc 1995;384:79.
[16] Wang CT, Clemens BM, White RL. IEEE Trans Magn 1996;32:4752.
[17] Muramatsu K, Yamaki TO, Matsuoka N, Takeuchi M, Matsumura Y, Uchida H. J Alloys Compd 2006;408:335.
[18] Luborsky FE. Amorphous metallic alloys. Ed. Butterworths; 1983.
[19] Buschow KHJ, Dirks AG. J Phys D: Appl Phys 1980;13:251.